
Dust evolution processes constrained by extinction curves in nearby galaxies

Kuan-Chou Hou^{1,2}, Hiroyuki HIRASHITA¹ and Michał J. MICHAŁOWSKI³

¹Institute of Astronomy, and Astrophysics, Academia Sinica, PO Box 23-141, Taipei 10617, Taiwan

²Department of Physics, Institute of Astrophysics, National Taiwan University, Taipei 10617, Taiwan

³SUPA, Institute for Astronomy, University of Edinburgh, Royal Observatory, Blackford Hill, Edinburgh, EH9 3HJ, UK

*E-mail: kchou@asiaa.sinica.edu.tw

Received ; Accepted

Abstract

Extinction curves, especially those in the Milky Way (MW), the Large Magellanic Cloud (LMC), and the Small Magellanic Cloud (SMC), have provided us with a clue to the dust properties in the nearby Universe. We examine whether or not these extinction curves can be explained by well known dust evolution processes. We treat the dust production in stellar ejecta, destruction in supernova shocks, dust growth by accretion and coagulation, and dust disruption by shattering. To make a survey of the large parameter space possible, we simplify the treatment of the grain size distribution evolution by adopting the ‘two-size approximation’, in which we divide the grain population into small ($\lesssim 0.03 \mu\text{m}$) and large ($\gtrsim 0.03 \mu\text{m}$) grains. It is confirmed that the MW extinction curve can be reproduced in reasonable ranges for the time-scale of the above processes with a silicate-graphite mixture. This indicates that the MW extinction curve is a natural consequence of the dust evolution through the above processes. We also find that the same models fail to reproduce the SMC/LMC extinction curves. Nevertheless, this failure can be remedied by giving higher supernova destruction rates for small carbonaceous dust and considering amorphous carbon for carbonaceous dust; these modification fall in fact in line with previous studies. Therefore, we conclude that the current dust evolution scenario composed of the aforementioned processes is successful in explaining the extinction curves. All the extinction curves favor efficient interstellar processing of dust, especially, strong grain growth by accretion and coagulation.

Key words: methods: analytical — dust, extinction — galaxies: evolution — galaxies: ISM — Galaxy: evolution — Magellanic Clouds

1 Introduction

Dust enrichment is one of the most important aspects for understanding the evolution of galaxies. Dust absorbs and scatters the stellar light and reemits it in the far infrared, thereby shaping the spectral energy distribution (SED) (e.g. Yajima et al. 2014; Schaerer et al. 2015, for recent modeling). The surface of dust grains provides a condition suitable for efficient forma-

tion of molecular hydrogen, which is an important coolant in low-metallicity clouds (e.g. Cazaux & Spaans 2004). Dust itself is also an important coolant in star formation, inducing the final fragmentation to determine the stellar mass (Omukai et al. 2005; Schneider et al. 2006).

For the important role of dust in determining the SED of galaxies, the wavelength dependence of extinction (extinction

is the sum of absorption and scattering), the so-called extinction curve, is the central quantity. Moreover, extinction curves reflect grain size distribution and grain composition (e.g. Weingartner & Draine 2001), both of which are important in determining the aforementioned processes, i.e. grain surface reactions and dust cooling (Yamasawa et al. 2011).

Because of the proximity, the most detailed studies of extinction curves have been performed in the Milky Way (MW), the Large Magellanic Cloud (LMC), and the Small Magellanic Cloud (SMC), where the foreground extinction for each individual bright stellar source can be measured (e.g. Pei 1992; Gordon et al. 2003). There have been various theoretical efforts of explaining these extinction curves through the modeling of grain composition and size distribution. Mathis, Rumpl & Nordsieck (1977, hereafter MRN) showed that a mixture of silicate and graphite with a grain size distribution of a power law $\propto a^{-3.5}$ (a is the grain radius and they considered ($a \sim 0.005\text{--}0.25 \mu\text{m}$)) reproduces the MW extinction curve (see also Kim, Martin & Hendry 1994), Pei (1992) showed that the extinction curves in the LMC and SMC are also explained by the same grain size distribution with different abundance ratios between silicate and graphite. Weingartner & Draine (2001) applied more detailed functional forms of grain size distributions to explain the extinction curves in the MW, LMC, and SMC. Although these models are successful in explaining the extinction curves, we still need to clarify how such grain size distributions as assumed in their models are established as a consequence of dust evolution in galaxies.

There have been some efforts of modeling the evolution of grain size distribution in galaxies. Liffman & Clayton (1989) treated the evolution of grain size distribution by considering the formation of refractory dust in stellar ejecta, the growth of mantles in the dense medium, and dust destruction in supernova shocks. Although their efforts of treating the grain size distribution is pioneering, their method based on tracing individual particles cannot treat grain fragmentation (or shattering) and grain sticking (or coagulation). O'Donnell & Mathis (1997) incorporated coagulation, shattering, and shock destruction for the dust processing mechanisms and roughly reproduced the MW extinction curve by the grain size distribution calculated in their models. Their results indicate the importance of these grain processing mechanisms in explaining the extinction curve. However, they only discussed the condition specific for the current MW, and the question still remains as to whether or not the MW extinction curve is reproduced as a result of dust evolution, which is coupled with the dust enrichment history of the MW. Moreover, the different shapes of extinction curves in the LMC and SMC still need to be addressed.

Recently, the evolution of grain size distribution has been formulated in a consistent manner with galaxy evolution. Asano et al. (2013) constructed a framework for treating the evolu-

tion of grain size distribution over the entire galaxy history. In their calculation, dust formed in stellar ejecta, that is, supernovae (SNe) and asymptotic giant branch (AGB) star winds, dominate the grain size distribution at the early stage of galactic evolution (Bianchi & Schneider 2007; Nozawa et al. 2007; Valiante et al. 2009; Gall et al. 2011; Yasuda & Kozasa 2012). Asano et al. (2013) assumed that these stellar sources form large ($\sim 0.1 \mu\text{m}$) grains, based on theoretical and observational evidence (see section 2.1 of H15 and Section 2.1 of the present paper). Thus, the dust is dominated by large grains at the early stage of galaxy evolution. As the system is enriched with dust, shattering as a result of grain–grain collision becomes efficient enough to increase the abundance of small grains. The increase of small grains drastically enhances the total grain surface area; as a consequence, grain growth by the accretion of gas-phase metals becomes the most important process for dust enrichment. Afterwards, the abundant small grains coagulate to form large grains. Throughout the galaxy evolution, dust destruction by SN shocks in the ISM is the main loss mechanism of dust mass (see also Dwek & Scalo 1980). Asano et al. (2014) calculated the evolution of extinction curve based on their model of grain size distribution. Their results tend to predict steeper extinction curves than the MW curve because grain growth by accretion drastically increases the abundance of small grains. Nozawa et al. (2015) showed, however, that the MW extinction curve is reproduced by considering dense molecular clouds in which strong coagulation converts small grains to large grains and flattens the extinction curve. Their model also explains the extinction curves observed in high-redshift quasars.

Although the above recent models took into account the full details of grain formation and processing mechanisms, there are still some uncertain free parameters regarding the time-scales of individual processes. In particular, the time-scales (or efficiencies) of accretion, shattering, and coagulation are strongly affected by the density structures in the ISM, since accretion and coagulation work only in the dense and cold ISM while shattering occurs predominantly in the diffuse ISM (Asano et al. 2013). Therefore, to complement their detailed models, a parameter survey study is desirable; that is, we need to survey all the reasonable ranges of the time-scales, for the purpose of checking if their conclusions are sensitive to the assumed time-scales or for the purpose of finding the ranges of the time-scales that reproduce successfully the observed extinction curves. However, their model based on a full treatment of grain size distribution requires a lot of computational time, and is not suitable for such a parameter survey study.

To make a parameter survey possible in a reasonable computational time, we adopt a simplified model developed by Hirashita (2015, hereafter H15) to calculate the evolution of grain size distribution: they adopted a ‘two-size approximation’ approach, in which the grain sizes are represented by two sizes:

large ($\gtrsim 0.03 \mu\text{m}$) and small ($\lesssim 0.03 \mu\text{m}$) grains. The model includes all the above processes considered by Asano et al. (2013) but only treat the mass exchange between the small and large grain populations. H15 showed that this two-size approximation traces the same evolutionary behaviors of grain size distribution and extinction curve as presented in Asano et al. (2013) and Asano et al. (2014). Therefore, H15 concluded that the two-size approximation can be used as a simplified (or computationally cheap) version of the full treatment of grain size distribution.

Using this two-size approximation with two dust species, silicate and graphite, Bekki et al. (2015) investigated the SMC/LMC extinction curves with a framework of a one-zone chemical evolution. They proposed a scenario in which small graphite grains are transported out of the galaxy in the latest starburst in the SMC (probably by radiation pressure), reproducing the SMC extinction curve, which does not show a 2175 Å bump caused by small graphite grains. This scenario that small graphite grains are selectively lost by dust wind reproduces the LMC extinction curve as well. However, it is yet to be proven that radiation pressure is effective in selective transport of small carbonaceous dust.

Although the above dust wind scenario can reproduce the extinction curves, it is still worth considering if dust processing mechanisms that work within a galaxy explain the extinction curves. In other words, how well the interstellar dust processing could reproduce the MW, LMC, and SMC extinction curves is still to be clarified. In this paper, therefore, we use the dust evolution model based on the two-size method developed in H15 and survey reasonable ranges of parameters characterizing the time-scales of individual dust processing mechanisms. We compare the extinction curves calculated by our models with those observed in the MW, LMC and SMC, and examine if these observed extinction curves can be reproduced by the models. In addition, we will be able to constrain the time-scales of dust processing mechanisms that govern the grain size distribution. The simplicity of the two-size approach enables us to fully survey the reasonable ranges of individual time-scales for the first time. We also discuss a possibility that the extinction curves of these three galaxies are simultaneously explained with a single evolutionary scenario of dust evolution.

This paper is organized as follows. In Section 2, we describe the dust enrichment model and the calculation method of extinction curves. In Section 3, we show the calculated extinction curves, which are compared with the observed extinction curves in the MW, LMC, and SMC. We discuss the results, laying particular emphasis on the time-scales of various dust processing mechanisms. Finally, we provide the conclusions in Section 5.

2 Dust enrichment model

We use the two-size dust enrichment model developed by H15. In this model, the dust grains are divided into small and large grains, considering that various grain processing mechanisms work differently between these two grain populations. H15 proposed $a = 0.03 \mu\text{m}$, where a is the grain radius, for the boundary between the two populations based on the full grain size calculations by Asano et al. (2013), whose models have been successful in explaining the extinction curves in the MW and high-redshift galaxies (Nozawa et al. 2015). The model takes into account dust supply by stellar ejecta, dust destruction in supernova shocks, grain growth by accretion and coagulation and grain disruption by shattering. As formulated in Bekki et al. (2015), we also separately solve silicate and carbonaceous dust. These two species are often adopted to explain extinction curves (e.g. Weingartner & Draine 2001). Since the model successfully explained the dust abundance in nearby galaxies in H15, we concentrate on extinction curves, which reflect grain size distributions, in this paper. Below we explain the models. We adopt $Z_{\odot} = 0.02$ for the solar metallicity throughout this paper following H15.

2.1 Two-size, two-species model

In H15, different dust species (i.e. silicate and carbonaceous dust) were not treated separately. In this paper, since dust material properties are important in reproducing extinction curves, we solve the evolution of different species, silicate and carbonaceous dust, separately. We represent silicate and carbonaceous dust by the evolution of Si and C, and assume that the mass fraction of Si in silicate is 0.166 while that of C in carbonaceous dust is 1. After applying the instantaneous recycling approximation (Tinsley 1980), the dust enrichment equations of each species for large and small grains are written as (see H15 for the derivation)

$$\begin{aligned} \mathcal{Y}_X \frac{d\mathcal{D}_{1,X}}{dZ} &= f_{\text{in},X}(\mathcal{R}Z + \mathcal{Y}_X) + \beta_{\text{co}}\mathcal{D}_{s,X} - (\beta_{\text{SN}} + \beta_{\text{sh}} + \mathcal{R})\mathcal{D}_{1,X}, \\ \mathcal{Y}_X \frac{d\mathcal{D}_{s,X}}{dZ} &= \beta_{\text{sh}}\mathcal{D}_{1,X} - \left(\frac{\beta_{\text{SN}}}{\alpha_X} + \beta_{\text{co}} + \mathcal{R} - \beta_{\text{acc}} \right) \mathcal{D}_{s,X}, \end{aligned} \quad (2)$$

where subscript X indicates the dust species (Si and C), $\mathcal{D}_{s,X}$ and $\mathcal{D}_{1,X}$ are the dust-to-gas ratios of small grains and large grains, respectively, $f_{\text{in},X}$ is the dust condensation efficiency of element X in the stellar ejecta, \mathcal{R} is the returned mass fraction from the formed stars, \mathcal{Y}_X is the mass fraction of newly produced element X, α_X is the enhancement factor of SN destruction for small grains relative to large grains, and β_{SN} , β_{sh} , β_{co} and β_{acc} indicate the efficiencies (explained below) of supernova destruction, shattering, coagulation and accretion, respectively. Note that these efficiencies (β s) depend on $\mathcal{D}_{i,X}$ ($i = s$ or l) except β_{SN} (see below). Thus, β s depend on material X, although we do not express this dependence explicitly for the

brevity of notation.

Now we explain equations (1) and (2) briefly. Equation (1) describes the increase of large grains. The right-hand size of this equation represents the stellar dust production [$f_{\text{in},X}(\mathcal{R}Z + \mathcal{Y}_X)$], the increase by coagulation of small grains ($\beta_{\text{co}}\mathcal{D}_{s,X}$), the decreases by SN destruction and shattering ($\beta_{\text{SN}}\mathcal{D}_{l,X}$ and $\beta_{\text{sh}}\mathcal{D}_{l,X}$, respectively), and the dilution of dust-to-gas ratio by returned gas from stars ($\mathcal{R}\mathcal{D}_{l,X}$). Equation (2) shows the increase of small grains, and it includes similar terms to equation (1). Note that the shattering and coagulation terms in equation (2) have the opposite sign to those in equation (1), since shattering is source and coagulation is sink for small grains. The increase of dust abundance by accretion ($\beta_{\text{acc}}\mathcal{D}_{s,X}$) only appears in equation (2); indeed, grain growth by accretion is much more efficient for small grains than for large grains because small grains have much larger surface-to-volume ratio (Hirashita & Kuo 2011; Asano et al. 2013; H15).

The reason why we assume that stellar ejecta provide large grains in both SNe and AGB star winds is based on several theoretical and observational studies. For observational evidence, Gall et al. (2014) obtained the infrared spectrum of SN 2010jl, suggesting that newly formed dust in SN ejecta is dominated by large grains. Scicluna et al. (2015) showed with imaging polarimetry at optical and near-infrared wavelengths that the grains radii in the wind of a red supergiant star VY Canis Majoris is on average $\sim 0.5 \mu\text{m}$. The typical size of grains produced by AGB stars is also suggested to be large ($a > 0.1 \mu\text{m}$) from observations of SEDs (Groenewegen 1997; Gauger et al. 1999), and also the polarization observation done by Norris et al. (2012) supports large sizes of dust grains produced by AGB stars. Several theoretical studies showed that reverse shocks more efficiently destroy small grains than large grains, which makes dust grains produced by SNe biased to large sizes (Nozawa et al. 2007; see also Bianchi & Schneider 2007; Marassi et al. 2015). Theoretical studies have also shown that dust grains formed in AGB star winds have large sizes (Yasuda & Kozasa 2012; Ventura et al. 2012). There is also evidence from meteoritic samples that dust species such as SiC and graphite, whose isotopic compositions indicate AGB star origin, have large grain sizes ($a \gtrsim 0.1 \mu\text{m}$), supporting the formation of large grains in AGB stars (e.g., Amari, Lewis, & Anders 1994; Hoppe & Zinner 2000). These results robustly indicate that the sizes of grains originating from stellar sources are biased to large sizes compared with the ISM grains; as long as this is true, it is enough to include stellar dust production only in equation (1) for the purpose of this paper. Moreover, if interstellar processing is more important than stellar sources, the detailed assumption on the grain size distribution of stellar dust is not essential.

We evaluate β s as follows: $\beta_{\text{SN}} \equiv \tau_{\text{SF}}/\tau_{\text{SN}}$, $\beta_{\text{sh}} \equiv \tau_{\text{SF}}/\tau_{\text{sh}}$ and $\beta_{\text{co}} \equiv \tau_{\text{SF}}/\tau_{\text{co}}$, where $\tau_{\text{SF}} \equiv M_{\text{gas}}/\psi$ (M_{gas} is the total gas

mass in the galaxy and ψ is the star formation rate) is the star formation time-scale, and the shattering and coagulation time-scales are written as

$$\tau_{\text{sh}} = \tau_{\text{sh},0} \left(\frac{\mathcal{D}_{l,X}}{\mathcal{D}_{\text{MW},l}} \right)^{-1}, \quad (3)$$

and

$$\tau_{\text{co}} = \tau_{\text{co},0} \left(\frac{\mathcal{D}_{s,X}}{\mathcal{D}_{\text{MW},s}} \right)^{-1}, \quad (4)$$

where the time-scales are normalized to $\tau_{\text{sh},0}$ and $\tau_{\text{co},0}$ at the MW dust-to-gas ratio, $\mathcal{D}_{\text{MW},l} = 0.007$ and $\mathcal{D}_{\text{MW},s} = 0.003$ (H15). Since shattering and coagulation are collisional processes, their time-scales are inversely proportional to the dust-to-gas ratio of the relevant species. The accretion efficiency β_{acc} is regulated by the lifetime of dense clouds (τ_{cl}), which host grain growth by accretion: accretion is more efficient if τ_{cl} is longer and metallicity is higher. In the calculation of β_{acc} , we also need atomic mass m_X , metal abundance (X/H) normalized to solar abundance [$(X/H)_{\odot}$], mass fraction of key species f_X as given in Table 1 (Hirashita & Kuo 2011; H15). We adopt $\alpha_X = 1$ unless otherwise stated (we will vary α_X for the SMC and LMC later).

To model the evolution of the two species (silicate and carbonaceous dust) separately, we also need to estimate the fraction of newly produced metals (\mathcal{Y}_X) and the dust condensation efficiency ($f_{\text{in},X}$) for C and Si, by adopting the same yield data as in Asano et al. (2013). We adopt the metal and dust yields of AGB stars for a range of progenitor mass at the zero-age main sequence, $m = 1-8 M_{\odot}$ from Karakas (2010) and Zhukovska et al. (2008), respectively, and the metal and dust yields of SNe for $m = 8-40 M_{\odot}$ from Kobayashi et al. (2006) and Nozawa et al. (2007, with hydrogen number density 1 cm^{-3} and the unmixed helium core). For a given metallicity, Z , \mathcal{Y}_X and $f_{\text{in},X}$ are evaluated as

$$\mathcal{Y}_X = \int_{m_t}^{40 M_{\odot}} m_{Z,X}(m) \phi(m) dm, \quad (5)$$

and

$$f_{\text{in},X} = \frac{\int_{m_t}^{40 M_{\odot}} m_{d,X}(m) \phi(m) dm}{\int_{m_t}^{40 M_{\odot}} m_{Z,X}(m) \phi(m) dm}, \quad (6)$$

where m_t is the turn-off mass at galaxy age t , $\phi(m)$ is the stellar initial mass function (IMF), $m_{Z,X}(m)$ is the total mass of newly produced element X as a function of m , and $m_{d,X}$ is the mass of newly produced element X condensed into dust as a function of m . Because \mathcal{Y}_X and $f_{\text{in},X}$ are much less sensitive to Z than to m , the values averaged for metallicity between $0.01 Z_{\odot}$ and $1 Z_{\odot}$ are used for simplicity (see Fig. 1). The values of \mathcal{Y}_X and $f_{\text{in},X}$ are listed in Table 1. We adopt a Salpeter IMF [$\phi(m) \propto m^{-2.35}$] with a stellar mass range of $0.1-100 M_{\odot}$. We integrate the metal and dust yields up to $40 M_{\odot}$, assuming that stars heavier than $40 M_{\odot}$ do not eject any mass into the ISM

(Heger et al. 2003). The returned fraction is estimated as

$$\mathcal{R} = \int_{m_t}^{40 M_{\odot}} [m - w(m)] \phi(m) dm, \quad (7)$$

where the remnant mass, $w(m)$, is adopted from the fitting formula provided by Inoue (2011). We adopt $\mathcal{R} = 0.25$, the same value as in our previous work (H15; see also Appendix A in Hirashita & Kuo 2011).

In Fig. 2, we show the dependence of metallicity-averaged \mathcal{Y}_X and $f_{in,X}$ on the age t (or m_t). We observe that the change of those parameters with the age is within a factor of 2 as long as $t \gtrsim 10^9$ yr. This means that, as long as we are interested in the MW, LMC, and SMC, whose stellar mass has built up over the time comparable to the cosmic age ($t \gtrsim 10^9$ yr), the results are not sensitive to the choice of m_t . Thus, we assume the constant values listed in Table 1 for \mathcal{Y}_X and $f_{in,X}$, where we choose the turn-off mass $m_t = 1 M_{\odot}$.

The dust yield adopted above may still be uncertain. Alternative dust yield data are available in Bianchi & Schneider (2007) for SNe and Ventura et al. (2012) for AGB stars. In fact, the shape of extinction curve is not affected by the detailed choice of dust yield because of the following reason. If the dust formation is dominated by stellar sources, the extinction curve is flat, since we assume that stars produce only large grains. Thus, the dust composition is of second importance in determining the shape of extinction curve. If the grain size distribution is governed by interstellar processing (i.e. processes other than stellar dust formation), the fraction of metals locked into dust is not determined by $f_{in,X}$ any more but is dominated by accretion and destruction (Inoue (2011); H15). Therefore, adopting other dust yield data does not affect our conclusion in this paper.

2.2 Extinction curve

The whole range of grain size is represented by only two populations (large and small grains), while the grain size distribution itself is necessary in calculating extinction curves. Thus, in order to calculate extinction curves in the framework of two-size approximation, we still need to assume a specific functional form for the grain size distribution, as a result of a trade-off between the simplicity of the two-size approximation and the detailed treatment of grain size distribution. Following H15, we adopt a modified-lognormal function for the grain size distribution:

$$n_{i,X}(a) = \frac{C_{i,X}}{a^4} \exp \left\{ -\frac{[\ln(a/a_{0,i})]^2}{2\sigma^2} \right\}, \quad (8)$$

where subscript i indicates the small ($i=s$) or large ($i=l$) grain component, C_i is the normalization constant and $a_{0,i}$, and σ are the central grain radius and the standard deviation, respectively. We adopt $a_{0,s} = 0.005 \mu\text{m}$, $a_{0,l} = 0.1 \mu\text{m}$ and $\sigma = 0.75$, and determine the normalization constants by

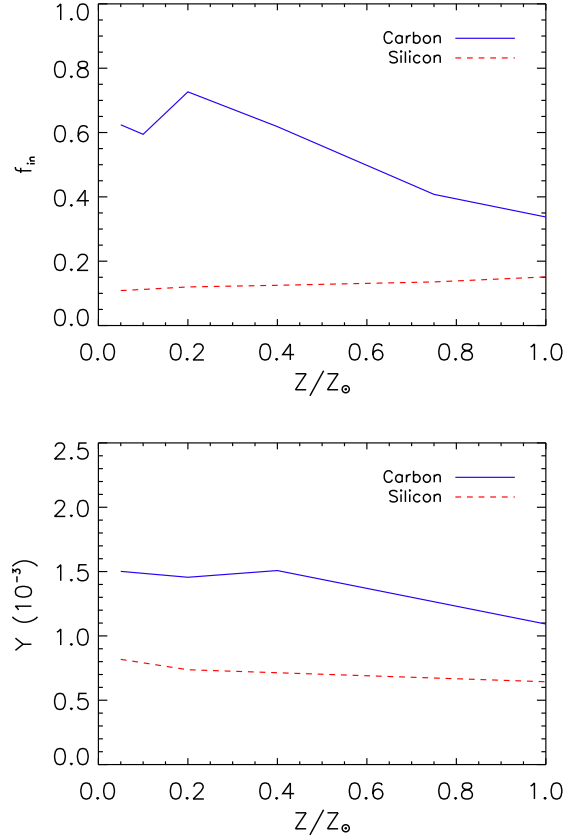


Fig. 1. Upper panel: Dust condensation efficiency $f_{in,X}$ as a function of metallicity Z . Bottom panel: Mass fraction of newly produced metal \mathcal{Y}_X as a function of metallicity Z . In both panels, solid and dashed lines indicate carbon and silicon, respectively.

$$\mu m_H \mathcal{D}_{i,X} = \int_0^{\infty} \frac{4}{3} a^3 \rho_X n_{i,X}(a) da, \quad (9)$$

where $\mu = 1.4$ is the gas mass per hydrogen nucleus, m_H is the mass of hydrogen atom and ρ_X is the material density of dust grains (given in Table 1). H15 confirmed that, if the small-to-large grain abundance ratio is the same as the MRN grain size distribution, the above functional form correctly reproduces the MW extinction curve. Weingartner & Draine (2001) made more efforts of precise fitting to the MW extinction curve. Although the detailed functional form is different, their size distributions for the mean MW extinction curve still have mass ratios of large grains to small grains which are similar to the MRN size distribution. It is worthy pointing out that the peaks of the two log-normal components are located at similar grain sizes to the two peaks in the graphite grain size distribution of Weingartner & Draine (2001).

The extinction at wavelength λ in units of magnitude ($A_{\lambda,X}$) normalized to the column density of hydrogen nuclei (N_H) is written as

Table 1. Adopted quantities.

| Species | X | f_X | m_X (amu) | $(X/H)_\odot$ | ρ_X (g cm $^{-3}$) | $f_{in,X}$ | \mathcal{Y}_X |
|-------------------|----|-------|-------------|-----------------------|--------------------------|------------|-----------------------|
| Carbonaceous dust | C | 1 | 12 | 2.88×10^{-4} | 2.24^a | 0.55 | 1.38×10^{-3} |
| Silicate | Si | 0.166 | 28.1 | 4.07×10^{-5} | 3.5 | 0.13 | 7.3×10^{-4} |

^aAmorphous carbon is introduced for the fitting of the SMC/the LMC extinction curves, using $\rho_C = 1.81$ g cm $^{-3}$ (Zubko et al. 2004).

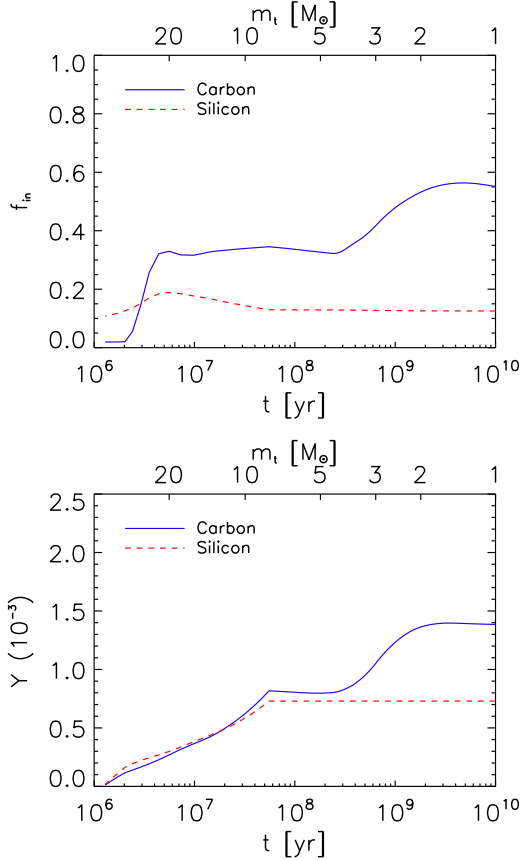


Fig. 2. Upper panel: Dependence of the dust condensation efficiency $f_{in,X}$ on the age/the turn-off mass. Bottom panel: Dependence of the mass fraction of newly produced metals \mathcal{Y}_X on the age/the turn-off mass. In both panels, solid and dashed lines indicate carbon and silicon, respectively.

$$\frac{A_{\lambda,X}}{N_H} = 2.5 \log_e \sum_i \int_0^\infty n_{i,X}(a) \pi a^2 Q_{ext}(a, \lambda, X), \quad (10)$$

where $Q_{ext}(a, \lambda, X)$ is the extinction coefficient (extinction cross section normalized to the geometric cross section) as a function of grain size, wavelength and species. The total extinction A_λ is calculated by summing $A_{\lambda,X}$ for all the species. We calculate $Q_{ext}(a, \lambda, X)$ using the Mie theory (Bohren & Huffman 1983) based on the same optical constants for silicate and graphite in Weingartner & Draine (2001). All the grains are assumed to be spherical with uniform composition. For the SMC and LMC, we introduce amorphous carbon (AC) for carbonaceous dust as a representative carbonaceous species without the 2175 Å feature, and the extinction coefficient of amor-

phous carbon is calculated with the optical constants provided by Zubko et al. (1996) (their ‘ACAR’ is adopted).

2.3 Observational data for extinction curves

In order to judge whether or not the calculated extinction curves successfully explain the observed extinction curves, we compare the extinction curve shape, which is defined as A_λ/A_V (the wavelength at the V band is $0.55 \mu\text{m}$). We introduce Δ^2 to measure the ‘distance’ between the calculated and observed extinction curves:

$$\Delta^2 = \sum_i [(A_{\lambda_i}/A_V)_{\text{model}} - (A_{\lambda_i}/A_V)_{\text{obs}}]^2, \quad (11)$$

where the subscripts ‘model’ and ‘obs’ indicate the model and the observational values, respectively, and the sum is taken for all the sampled wavelengths λ_i .

The observed extinction curves are taken from Pei (1992). The extinction curves are given at 30 wavelengths from ultraviolet (UV) to near IR. These wavelengths are used for λ_i above. Fitzpatrick & Massa (2007) presented extinction curves along various line of sights in the MW. Since these extinction curves show a dispersion as quantified by Nozawa & Fukugita (2013), we will later use the dispersion to define a ‘reasonable’ range for the above distance Δ^2 .

We surveyed the appropriate parameter ranges listed in Table 2, which follows the values suggested in H15. H15 suggested these ranges based on previous theoretical dust evolution studies and confirmed that they reproduce the relation between dust-to-gas ratio and metallicity in nearby galaxies. Each model with a certain set of parameters produces the dust-to-gas ratio $\mathcal{D}_{i,X}$ as a function of metallicity Z . We calculate the extinction curve using the calculated $\mathcal{D}_{i,X}$ at the metallicity appropriate for each galaxy. In this paper, we assume the metallicities of the MW, LMC and SMC to be $1 Z_\odot$, $0.5 Z_\odot$ and $0.2 Z_\odot$, respectively (Russell & Dopita 1992; Korn et al. 2000).

3 results

3.1 Dust-to-gas ratio

The parameter dependence of the evolution of dust-to-gas ratio has already been investigated in H15. We only show an example of the evolution of dust-to-gas ratio for the fiducial parameter values given in Table 2 (see Section 3.2 for the choice

Table 2. Parameter ranges surveyed.

| Process | Parameter | Minimum | Middle | Maximum |
|----------------|----------------------|------------------------------|----------------------------|-------------------------------|
| Star formation | τ_{SF} | $5 \times 10^8 \text{ yr}^*$ | $5 \times 10^9 \text{ yr}$ | $5 \times 10^{10} \text{ yr}$ |
| Shattering | $\tau_{\text{sh},0}$ | 10^7 yr^* | 10^8 yr | 10^9 yr |
| Coagulation | $\tau_{\text{co},0}$ | 10^6 yr^* | 10^7 yr | 10^8 yr |
| Accretion | τ_{cl} | 10^6 yr | 10^7 yr | 10^8 yr^* |
| SN destruction | β_{SN} | 4.82 | 9.65* | 19.3 |

*Fiducial case (see Section 3.2).

of the fiducial parameter set). In Fig. 3, we show $\mathcal{D}_{1,X}$, $\mathcal{D}_{s,X}$, $\mathcal{D}_X (\equiv \mathcal{D}_{1,X} + \mathcal{D}_{s,X})$ and $\mathcal{D} (\equiv \mathcal{D}_C + \mathcal{D}_{Si})$ as a function of Z . At low metallicity, the dust production is dominated by the stellar sources (i.e. SNe and AGB stars), which are assumed to form large grains. At this stage, $\mathcal{D}_X \simeq f_{\text{in},X} Z$ until SN destruction is strong enough to suppress the increasing rate. This suppression by destruction is seen around $Z \sim 0.03 Z_\odot$ in Fig. 3. In the meantime, shattering continuously transforms large grains into small grains as seen in the initial rise of the small-to-large grain abundance ratio ($\mathcal{D}_{s,X}/\mathcal{D}_{1,X}$). Shattering is thus important for the first production of small grains. Subsequently, accretion efficiency increases the abundance of small grains as a consequence of the enhancement of grain surface area by shattering as well as the increase of metallicity (i.e. abundance of accreting materials; see also Dwek & Scalo 1980; Inoue 2011; Kuo & Hirashita 2012; Mattsson et al. 2014). The silicate abundance becomes greater than carbonaceous dust abundance at this epoch. The dust mass increase by accretion saturates after a significant fraction of gas-phase metals are consumed. Coagulation becomes active with the enhancement of small grain abundance; as a result of coagulation, the small-to-large grain abundance ratio decreases. We refer the interested reader to H15 for the detailed discussions on the evolution of dust-to-gas ratio and small-to-large grain abundance ratio.

3.2 Parameter dependence of extinction curve

For the MW extinction curve, we use the results for each set of parameters at metallicity $Z = Z_\odot$, which is appropriate for the MW, and calculate the extinction curve by adopting graphite and silicate for the dust species. The calculated MW extinction curves are compared with the observed curve (Pei 1992). We examine the parameter dependence of extinction curve in Fig. 4. To this aim, we first choose a set of parameters that roughly fits the observed MW extinction curve. This parameter set is referred to as the fiducial case (Table 2). Note that, as shown later, there are other sets of parameters that give satisfactory fitting to the MW extinction curve; thus, the aim of taking the fiducial parameters is only to clarify the dependence on the parameters. Fig. 4 shows the extinction curve for the fiducial parameter set

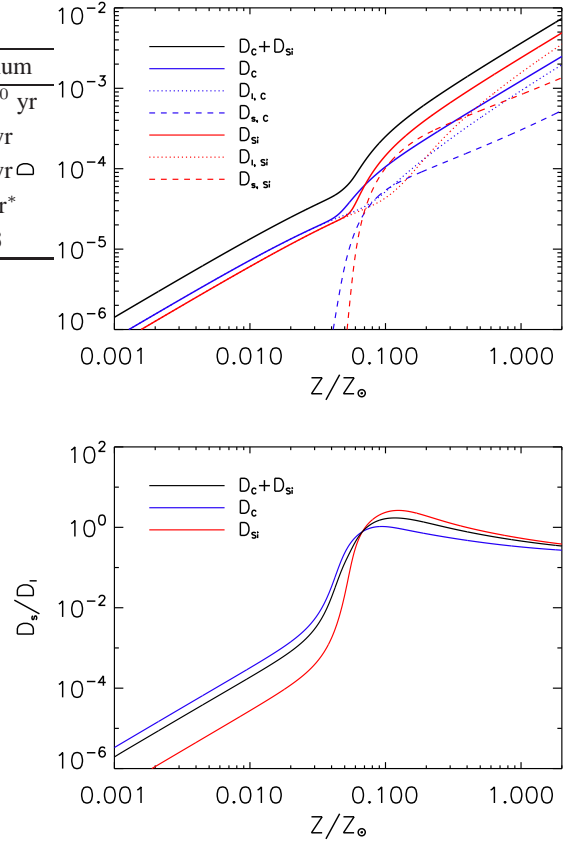


Fig. 3. Upper panel: Dust-to-gas mass ratio as a function of metallicity Z normalized to the solar metallicity. We show the dust-to-gas ratios of carbonaceous dust (blue lines) and silicate (red lines) separately and the small grain dust-to-gas ratio (dashed lines) and large grain dust-to-gas ratio (dotted lines). The black solid line shows the total dust-to-gas ratio. Bottom panel: Small-to-large grain abundance ratio as a function of metallicity Z . The colors are the same as in the upper panel.

along with the variation caused by the change of each individual parameter.

We observe that the extinction curves are sensitive to the star formation, coagulation and accretion time-scales. Although Fig. 4 shows just example cases, it represents a general trend of extinction curves with varying parameters. We focus on the 2175 Å bump and the UV slope as prominent signatures of extinction curves. In general, shorter star-formation and shattering time-scales (τ_{SF} and τ_{sh}), a longer coagulation time-scale (τ_{co}) and a longer cloud lifetime (τ_{cl}) produce the extinction curves with a more prominent bump and a steeper slope because the small-to-large grain abundance ratio is larger. Shorter τ_{sh} (high shattering efficiency) produces more small grains. Coagulation has an opposite effect: short τ_{co} means efficient conversion of small grains into large gains, which smears out the signatures of extinction curve. The abundance of small grains increases more efficiently in a condition of longer τ_{cl} , which makes a stronger bump and a steeper slope. Shorter τ_{SF} decreases both

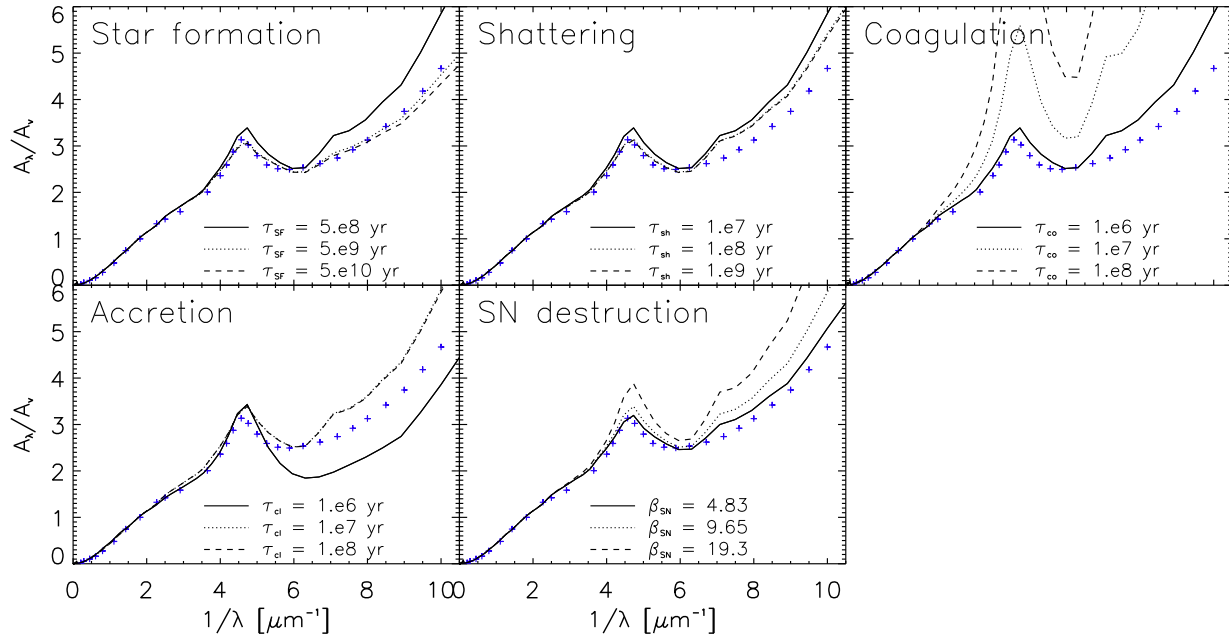


Fig. 4. Effect of each parameter on extinction curves. For the parameters other than the one specified in each panel, we adopt the fiducial values listed in Table 2. Cross symbols show the observed mean extinction curve of the MW taken from Pei (1992). Solid, dotted and dashed lines correspond to the value of the parameter listed in the legend in each panel.

shattering and coagulation efficiencies (note that β_{sh} and β_{co} are both proportional to τ_{SF} ; Section 2.1), but the effect of shattering appears more prominently since coagulation takes place only after shattering (Section 3.1). The SN destruction efficiency β_{SN} shows a minor effect compared to other parameters; however, α_X , enhancement factor of SN destruction for small grains, proves to be important when we model the SMC/LMC extinction curves later.

3.3 The MW

We examine the $3^5 = 243$ combinations of parameter values listed in Table 2. Among them, we choose the cases with small Δ^2 (equation 11) for satisfactory fits. We adopt $\Delta^2 \leq 8$ for the criterion of good fit. As shown below, if we choose the extinction curves satisfying this criterion, the calculated extinction curves are roughly within the observed dispersion of the extinction curves in the MW in various lines of sight. This criterion also empirically works for the LMC and SMC as shown below. Since this criterion is only empirically imposed, we also show all the calculated extinction curves satisfying the criterion to visually confirm that the extinction curves calculated are actually near to the observed one.

In Fig. 5, we plot all the model extinction curves satisfying the criterion $\Delta^2 \leq 8$. We also show the dispersions of the MW extinction curves in various lines of sight (Fitzpatrick & Massa 2007; Nozawa & Fukugita 2013). We observe that the extinction curves selected with $\Delta^2 \leq 8$ roughly have a comparable

dispersion to the observed ones. In other words, $\Delta^2 \leq 8$ can be regarded as an acceptable range for the MW condition. We overproduce the dispersion for the 2175 Å bump feature, but this could be improved by a slight inclusion of AC, which does not show the 2175 Å bump feature.

In total, 35 per cent of the parameter sets satisfy the criterion, which implies that our model successfully contains the processes and parameter ranges that are suitable for the MW condition. On the other hand, the fact that a large number of parameter sets can reproduce the MW extinction curve indicates degeneracy; that is, the dust evolution history that reproduces the MW extinction curve is not unique. Nevertheless, we will show later that there is some preferred parameter space, and we will discuss the characteristics of the parameter sets that satisfy the criterion in Section 4.2.

3.4 The SMC

The SMC extinction curve is very different from the MW curve in that it does not show a prominent 2175 Å bump, and the LMC extinction curve is intermediate between these two curves (e.g. Fitzpatrick 1985). Therefore, we examine the SMC extinction curve first, and model the LMC curve as an intermediate case later. There is one thing we should keep in mind. The 2175 Å bump is absent in the SMC bar region, but a weak bump exists in the SMC wing region (Gordon et al. 2003), which implies a spatial variation of carbonaceous material properties among graphite, AC, and polycyclic aromatic hydrocarbons (PAHs) (Li

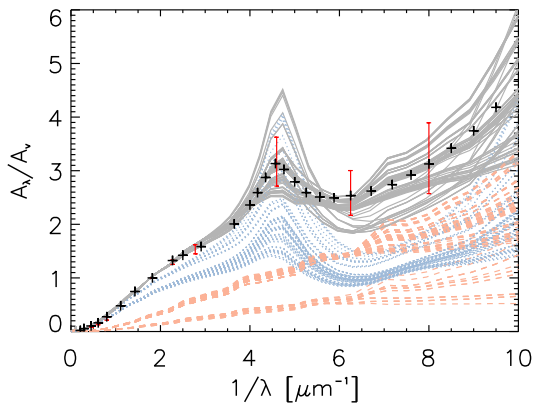


Fig. 5. Simulated MW extinction curves satisfying $\Delta^2 \leq 8$. Cross symbols are the same as in Fig. 4 and vertical bars are the 1σ dispersion taken from Fitzpatrick & Massa (2007). Gray lines present the total extinction curves, and blue dotted and orange dashed lines are the graphite and silicate component of extinction curves.

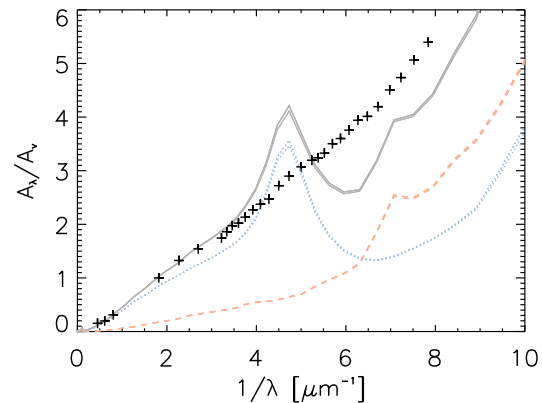


Fig. 6. Five best fitting extinction curves to the SMC with the same parameter sets and dust properties adopted for the MW. The crosses are the observed the SMC extinction curve taken from Pei (1992). All the models have $\Delta^2 > 8$, and thus the fit is not satisfactory. Lines and colors are the same as Fig. 5. Extinction curves are overlapping because of the degeneracy of parameters.

& Draine 2002). This variation may be driven by UV radiation (Jones 2009), but the mechanism of UV processing is not fully understood yet. In this paper, we do not include such processing explicitly, but simply focus on how the bumpless extinction curve is reproduced by a certain carbonaceous material.

We surveyed all the parameter sets and examined the goodness of fit for the SMC extinction curve at $Z = 0.2Z_\odot$ with the same dust species (silicate and graphite) as in the MW. However, we did not find any curve that satisfies $\Delta^2 \leq 8$. In Fig. 6, we show the five best fit models to the SMC extinction curve. The averaged Δ^2 for the best five fitting results (denoted as $\overline{\Delta^2}$) is $\overline{\Delta^2} = 15.8$.

As shown in Fig. 6, the largest discrepancy between the models and observation appears at UV wavelengths. The observed SMC extinction curve has no prominent 2175 Å bump feature and has a steep slope. In our models, the 2175 Å feature is due to small graphite grains and the steep UV slope is mostly due to small silicate grains. To reproduce the SMC extinction curves, thus, we propose two possible modifications: one is to use AC instead of graphite and the other is to increase the SN destruction efficiency for small carbonaceous grains (α_X in equation 2 with $X = C$). For the second solution, the 2175 Å bump feature should be suppressed while the steepness of the UV extinction curve should be kept, which indicates less small carbonaceous dust and enough small silicates; thus, we set $\alpha_C = 0.1$ to destroy small carbonaceous dust grains efficiently with $\alpha_{Si} = 1$ remaining the same to preserve small silicate grains. In the following, we examine these two possibilities.

3.4.1 AC

To solve the problem of the 2175 Å bump being too prominent, we introduce amorphous carbon (Zubko et al. 1996), a different

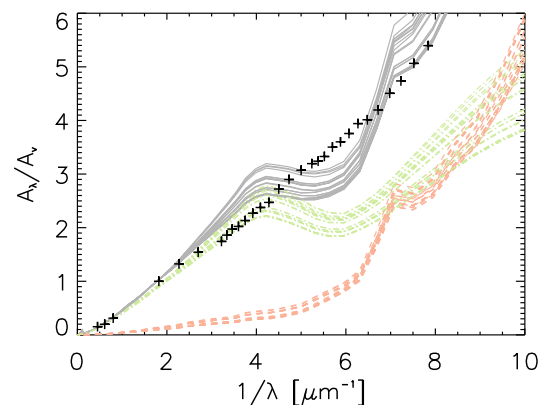


Fig. 7. Simulated SMC extinction curves satisfying $\Delta^2 \leq 8$ with adopting AC for carbonaceous dust. $\overline{\Delta^2} = 5.7$ and 10% parameter sets satisfy $\Delta^2 \leq 8$. The observational data points are the same as in Fig. 6. Gray lines present the total extinction curves, green dash-dotted and orange dashed lines are the AC and silicate component of extinction curves.

type of carbonaceous dust, which has no 2175 Å bump feature. The same material is also used by Nozawa et al. (2015) to explain the bumpless extinction curve of a high-redshift quasar. 10 per cent (25 parameter sets) of the 243 parameter sets satisfy $\Delta^2 \leq 8$. All these extinction curves with $\Delta^2 \leq 8$ are shown in Fig. 7. The extinction curves calculated with AC are closer to the observed SMC extinction curve than with graphite. However, AC still make a feature at wavelengths between 1,500 and 2,500 Å. The averaged Δ^2 for the five best fit results is $\overline{\Delta^2} = 5.7$, much smaller than the above (15.8). Therefore, using AC for carbonaceous dust improves the fit to the SMC extinction curve.

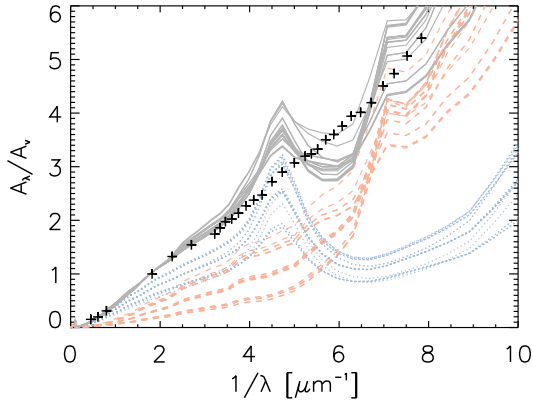


Fig. 8. Same as Fig. 7 but with $\alpha_C = 0.1$ and graphite for the carbonaceous species. $\overline{\Delta^2} = 4.0$ and 9% parameter sets satisfy $\Delta^2 \leq 8$. The observational data points are the same as in Fig. 6. Gray lines present the total extinction curves, and blue dotted and orange dashed lines are the graphite and silicate component of extinction curves.

3.4.2 $\alpha_C = 0.1$ with graphite

We propose a higher SN destruction efficiency for small carbonaceous dust grains than small silicates by introducing a small value of α_C to relatively suppress the abundance of small carbonaceous grains. This is motivated by the fact that the prominent 2175 Å bump is caused by small graphite grains: thus, we expect that the SMC extinction curve is better explained by the stronger destruction of small carbonaceous grains. Recall that we adopted $\alpha_X = 1$ for both carbonaceous dust ($X = C$) and silicate ($X = Si$) above. Here we give $\alpha_C = 0.1$ (an order of magnitude higher destruction rate for small carbonaceous dust) with $\alpha_{Si} = 1$ unchanged. Fig. 8 shows the extinction curves satisfying $\Delta^2 \leq 8$. We observe that the fitting is improved compared with the case of $\alpha_C = 1$, although the 2175 Å bump is still prominent. The bump remains prominent because accretion still contributes to enhancing the small grain abundance. We find 9 per cent (23 parameter sets) out of the 243 models satisfying $\Delta^2 \leq 8$. The average Δ^2 for the 5 best fit cases is $\overline{\Delta^2} = 4.0$, which is smaller than the above case; however, the persistence of bump indicates that enhancing the destruction of the bump carrier (small graphite grains in our case) is not a probable way of explaining the SMC extinction curve.

3.4.3 $\alpha_C = 0.1$ with AC

Adopting AC and the small $\alpha_C (= 0.1)$ at the same time, we calculate the extinction curve. We show the cases with satisfactory fit ($\Delta^2 \leq 8$) in Fig. 9. The average Δ^2 for the five best fitting cases is $\overline{\Delta^2} = 4.0$. Out of all the possible combinations of parameter values in Table 2, we find that 8 per cent, 20 parameter sets, of them satisfy $\Delta^2 \leq 8$. Although the percentage is not as high as the MW case, it is worth emphasizing that we find some satisfactory dust evolution models that fit the SMC

Table 3. Fitting to the SMC extinction curve with different model.

| Model | $\overline{\Delta^2}$ * | $\Delta^2 \leq 8$ ** |
|--------------------------------|-------------------------|----------------------|
| $\alpha_C = 1$ with graphite | 15.8 | 0 % |
| $\alpha_C = 1$ with AC | 5.7 | 10 % |
| $\alpha_C = 0.1$ with graphite | 4.0 | 9 % |
| $\alpha_C = 0.1$ with AC | 4.0 | 8 % |

* Average Δ^2 of 5 best fitting.

** Fraction of parameter sets satisfying $\Delta^2 \leq 8$.

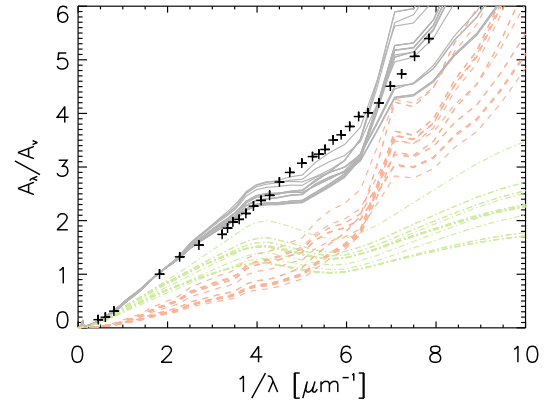


Fig. 9. Same as Fig. 7 but with $\alpha_C = 0.1$ and AC. We show not only the five best fits but also all the calculated curves satisfying $\Delta^2 \leq 8$. $\overline{\Delta^2} = 2.6$ and 11% parameter sets satisfy $\Delta^2 \leq 8$. The observational data points are the same as in Fig. 6. Gray lines present the total extinction curves, green dash-dotted and orange dashed lines are the AC and silicate component of extinction curves.

extinction curve with a common framework of dust enrichment. We discuss the properties of parameter sets giving the good fits in Section 4.2.

3.5 The LMC

Like the SMC case, the model with $\alpha_C = 1$ and using graphite for carbonaceous dust does not reproduce the LMC extinction curve at $Z = 0.5Z_\odot$. Because its 2175Å bump strength and UV slope are intermediate between the MW and SMC extinction curves, we treat the LMC as an intermediate case between the MW and SMC. We use the result at $Z = 0.5Z_\odot$, an appropriate ISM metallicity for the LMC (Russell & Dopita 1992). As intermediate values, we apply $\alpha_C = 0.2$ and a mixture of 50 per cent graphite and 50 per cent AC for the carbonaceous component with the silicate properties unchanged. We calculate the extinction curves for each parameter set, and show the extinction curves under the same criterion as the above ($\Delta^2 \leq 8$) for the LMC in Fig. 10. Among all the possible combinations of parameter values, we find that 27 per cent (66 parameter sets) of them satisfy the criterion.

The graphite fraction and α_C used for the fit of the extinction

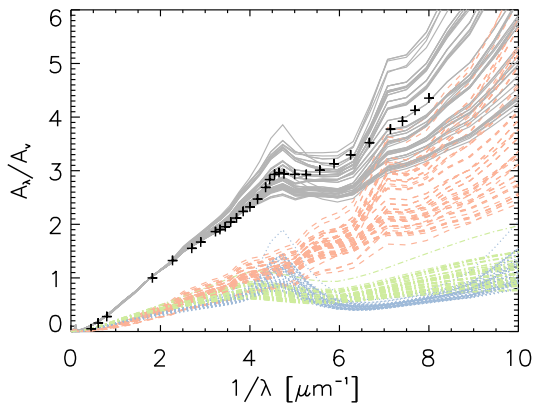


Fig. 10. Fit to the LMC extinction curve with $\alpha_C = 0.2$ and a mixture of 50 per cent graphite and 50 per cent AC for carbonaceous dust. The calculated curves satisfying $\Delta^2 \leq 8$ are shown. Cross symbols show the observed mean extinction curve of the LMC taken from Pei (1992). Gray lines present the total extinction curves, and blue dotted, green dash-dotted and orange dashed lines are the graphite, AC and silicate component of extinction curves.

Table 4. Tuned Parameters

| Galaxy | graphite %* | α_C | $\Delta^2 \leq 8^{**}$ |
|--------|-------------|------------|------------------------|
| MW | 100 | 1 | 35 % |
| LMC | 50 | 0.2 | 27 % |
| SMC | 0 | 0.1 | 8 % |

*Mass fraction of graphite for carbonaceous species. The rest is AC.

**Fraction of parameter sets satisfying $\Delta^2 \leq 8$.

curves in each galaxy is listed in Table 4 with the percentage of satisfactory fits. We hereafter adopt the graphite fraction and α_C in Table 4 for each galaxy.

4 discussion

4.1 Other possible dust species

Although some detailed dust models incorporating PAHs and other complicated dust species have been developed for extinction curves (Li & Draine 2001; Zubko et al. 2004; Draine & Li 2007), our conclusions by using only graphite and silicate still hold at least qualitatively because of the following reasons. Small graphite was classically introduced as being responsible for the 2175 Å bump but we can derive the same conclusion as long as the 2175 Å carrier is small grains. Steepness of far UV slope is mainly due to small silicate grains. The requirement of small grains for the UV slope robustly holds even if we adopt other grain species. Moreover, by construction of our models, we adopt the time-scales of various processes in a way independent of grain species. Therefore, our conclusion on the contributions from shattering, coagulation and accretion, which

determine the small-to-large grain abundance ratio still holds as long as this ratio shapes the extinction curves.

4.2 Constraint on the parameters

H15 showed that the dust-to-gas ratio produced by our model agrees with the relation between dust-to-gas ratio and metallicity of nearby galaxies. In this paper, thus, we have been concentrating extinction curves rather than dust abundance. Since the extinction curves calculated by our models directly reflect the parameters in our dust enrichment models, we here examine whether or not we can get useful constraints on those parameters through the observed extinction curves. In order to show the sensitivity to each parameter, we show the fraction of all the models that satisfy $\Delta^2 \leq 8$, which is used as a criterion of good fit. Because the time-scales of shattering and coagulation are degenerate with the star formation time-scale (Hirashita 2015), we use the $\beta_{sh,0}$ ($= \tau_{SF}/\tau_{sh,0}$) and $\beta_{co,0}$ ($= \tau_{SF}/\tau_{co,0}$) values to represent the effects of shattering and coagulation.

In Table 5, we show the percentage of the models satisfying the good-fit criterion with the specified parameter fixed and the others changed (over the three cases for each parameter) as shown in Table 2. For example, 21 per cent of the models show a satisfactory fit to the Milky Way extinction curve if the star-formation time-scale is fixed to $\tau_{SF} = 5 \times 10^8$ yr. In general, a higher percentage indicates that the fixed parameter value is more favored by the observed extinction curve. Among the processes, coagulation (β_{co}) and accretion (τ_{cl}) can be constrained most strongly. We find that weak coagulation with $\beta_{co} \leq 50$ does not reproduce the observed extinction curves for all the MW, LMC and SMC. We also observe that strong coagulation with $\beta_{co} = 5 \times 10^4$ find quite a large number of satisfactory fits while such a strong coagulation efficiency is less supported for the SMC. Since coagulation takes place only in the dense ISM (Hirashita & Yan 2009), this implies that the dense cloud fraction in the galaxy changes with different metallicities. Yet, even in the SMC, strong coagulation with $\beta_{co,0} \sim 5 \times 10^2 - 5 \times 10^3$ is favored. Necessity of strong coagulation to explain the MW extinction curve is consistent with more detailed dust evolution models in Asano et al. (2014) and Nozawa et al. (2015).

As also observed in Table 5, efficient accretion (larger $\tau_{cl} \sim 10^7 - 10^8$ yr) better explains the observed extinction curves in all the three galaxies. A long cloud lifetime ($\tau_{cl} = 10^8$ yr), that is, efficient accretion, is strongly favored for the SMC. The above results indicate that grain growth (accretion and coagulation) is a key process even at the SMC metallicity. Accretion is the most efficient mechanism of increasing the small grain abundance (H15), so that it provides the most natural way of explaining the steepness of the SMC extinction curve. As shown by Schneider et al. (2014) in comparison with the data taken by Gordon et al. (2014), it is possible that dust produced by stel-

lar sources explains the total dust budget in the LMC and SMC. However, as also mentioned by them, if we take dust destruction by SN shocks into account, an additional source of dust, such as accretion, would be required (see also Zhukovska & Henning (2013)). The importance of dust growth by accretion for the total dust abundance has already been shown for various galaxy samples by many authors (e.g. Dwek et al. 2007; Michałowski et al. 2010a, 2010b; Hirashita & Kuo 2011; Valiante et al. 2011; Kuo & Hirashita 2012; Mancini et al. 2015; Michałowski 2015). Recent experiments by Rouillé et al. (2014) showed that accretion actually occurs in cold environments.

Less models with a shorter SF time-scale ($\tau_{\text{SF}} = 5 \times 10^8$ yr) reproduce the observation extinction curve for all three galaxies than those with a longer τ_{SF} , which indicates that the MW, LMC and SMC have built up stars mildly on time-scales longer than 1 Gyr, and also implies that extinction curves might be influenced by the star formation history. Such a long τ_{SF} is consistent with the pictures adopted in other chemical evolution models (e.g. Bekki et al. 2015). For shattering and SN destruction, the parameter values we chose are equally favored by the observed extinction curves; in other words, it is difficult to constrain these parameters by the extinction curves. This is probably because the small and large grain abundances are overwhelmed by accretion and coagulation, respectively, with minor effects of the other processes.

To illustrate our results further, we make correlation plots between two parameters in Fig. 11. Each panel shows the relation between two parameters. For example, the upper right panel shows the constraints on the $\tau_{\text{cl}}-\beta_{\text{SN}}$ plane. Since we examine three values for each parameter, we have nine cases (nine grid points) in each panel. Each grid point shows one case with $\Delta^2 \leq 8$ with the two parameters fixed and the other three parameters moved (so there are 27 cases for each point); thus, if there are many points plotted, that combination of two parameter values has many cases that predict extinction curves close to the MW extinction curve. Larger symbols mean smaller values of Δ^2 (i.e. the calculated extinction curve is closer to the observed one if the symbol size is larger). For example, in the upper right panel, small τ_{cl} values (strong grain growth by accretion) is preferred by the Milky Way extinction curve, while β_{SN} is not constrained well (i.e. all the three values of β_{SN} are equally preferred). There are preferred trends for τ_{co} and τ_{cl} in such a way that strong coagulation and accretion accommodate more extinction curves close to the observed one. We observe almost no preference for the choice of τ_{sh} and β_{SN} . A longer τ_{SF} (mild star formation) is slightly favored than a shorter τ_{SF} (burst-like star formation). All these trends support the conclusions derived above as to Table 5. Fig. 11 also shows a diagonal trend in the $\tau_{\text{co}}-\tau_{\text{SF}}$ and $\tau_{\text{co}}-\tau_{\text{sh}}$ diagrams, which means that similar extinction curves are produced with similar values for ratio $\tau_{\text{co}}/\tau_{\text{SF}}$ or $\tau_{\text{co}}/\tau_{\text{sh}}$. This is because the coagulation

time-scale relative to the star formation time-scale is the real parameter that determines the grain size distribution, and the final small-to-large grain abundance ratio is determined by the balance between coagulation and shattering (see also H15). We obtained similar trends for preferred parameter ranges for the SMC and LMC as shown in Appendix 1.

4.3 Tuning for the SMC and LMC

To fit the observed SMC and LMC extinction curves, we introduced AC for carbonaceous dust and adopted a stronger SN destruction efficiency for small carbonaceous dust (α_{C}) (Sections 3.4 and 3.5). The key differences between the MW and SMC/LMC extinction curves are the strength of 2175 Å bump and the UV slope. Although the steep slope can be produced within the parameter ranges that we adopted, the lack of the 2175 Å bump feature cannot be explained as long as we adopt graphite for the carbonaceous component. We have also shown that, even if we impose a stronger destruction for carbonaceous dust than for silicate, the small carbonaceous grains are never eliminated because accretion is efficient enough to raise the abundance of small carbonaceous dust grains. Therefore, it was necessary to introduce AC instead of graphite for the purpose of explaining the SMC and LMC extinction curves.

It may be natural to assume an enhanced destruction efficiency also for silicate as well as carbonaceous dust. However, if we adopt $\alpha_{\text{Si}} = \alpha_{\text{C}} = 0.1$, the abundance ratio of carbonaceous dust to silicate does not change from the case of $\alpha_{\text{Si}} = \alpha_{\text{C}} = 1$, so that the feature caused by carbonaceous dust still remains prominently. Therefore, enhancing the destruction of small carbonaceous grains compared with that of small silicates is essential in explaining the extinction curves which lack prominent carbonaceous dust features.

Bekki et al. (2015) presented a different way of explaining the lack of the 2175 Å bump feature for the SMC extinction curve. In their models, a strong dust wind is assumed to be associated with the starburst events. Assuming that small graphite grains are easily removed by outflows, they indeed succeeded in reproducing the SMC and LMC extinction curves at the present age. Although their scenario is plausible, we have shown in this paper that modifications of the SN destruction efficiency and the introduction of AC without any dust outflow can also explain the SMC/LMC extinction curves.

Assuming AC to be the dominant carbonaceous dust component in the Magellanic Clouds may be observationally supported. It is indicated that the far-infrared SED of the LMC is produced by AC and silicate better than the standard graphite and silicate dust model (Meixner et al. 2010). Jones & Nuth (2011) mentioned that the lifetime of silicate is longer than that of AC, which would justify our different SN destruction rates between small silicate and AC grains. In this context, the small

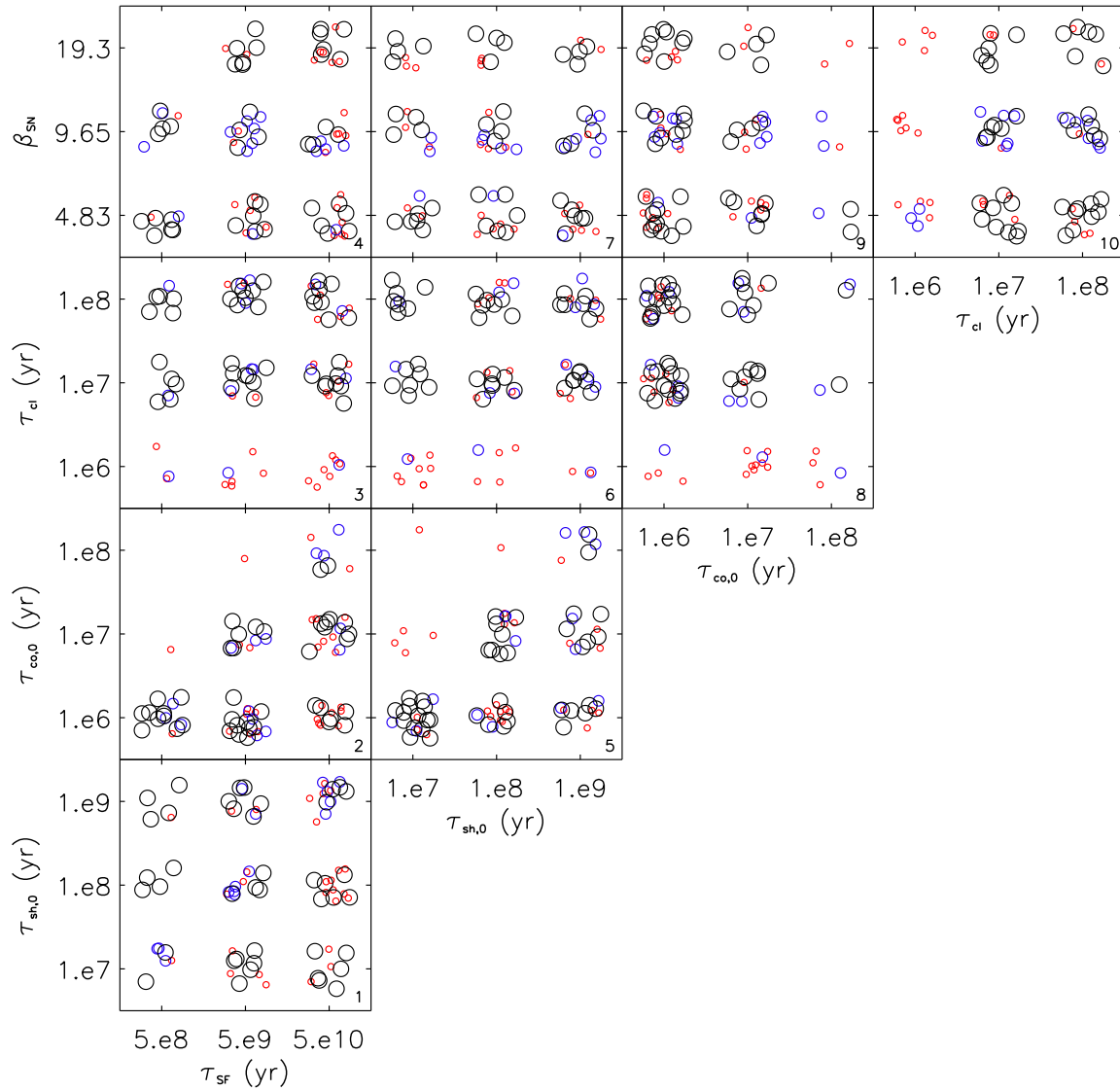


Fig. 11. Correlation plots between two parameters chosen in each panel for the MW case. Each parameter has three values; thus, each panel is composed of 9 grid points. Since the other three parameters are changed, we have 27 cases for each grid point. Among these 27 cases, we only show the cases with $\Delta^2 \leq 8$, each circle representing one case. To avoid overlaps of circles, we add a random offset for each circle. Symbol sizes correspond to values of Δ^2 : large black circles are for $\Delta^2 \leq 2$, medium blue circles are for $2 < \Delta^2 \leq 5$, and small red circles are for $5 < \Delta^2 \leq 8$. A grid point with many circles means that we find many cases that satisfy $\Delta^2 \leq 8$: thus, we regard the grid points with many large points are favored by the observed MW extinction curve. Panels showing $\tau_{\text{co},0}$ indicate that strong coagulation ($\tau_{\text{co},0} \leq 10^7$ yr) fits the observed data. Strong accretion ($\tau_{\text{cl}} \geq 10^7$) is also preferred. The relations between $\tau_{\text{co},0}$ and τ_{SF} and between $\tau_{\text{co},0}$ and $\tau_{\text{sh},0}$ show degeneracy in the diagonal direction. There are no clear constraints on τ_{sh} and β_{SN} .

Table 5. Fraction of calculated extinction curves that satisfies $\Delta^2 \leq 8$ and minimum Δ^2 under a given value of each fixed parameter.

| Milky Way | | | | | | | | | | | | | | |
|--------------------|----|------------------|--------------------|----|------------------|-----------------|----|------------------|------------------|----|------------------|--------------|----|------------------|
| τ_{SF} (yr) | % | Δ_{min}^2 | $\beta_{sh,0}$ | % | Δ_{min}^2 | $\beta_{co,0}$ | % | Δ_{min}^2 | τ_{cl} (yr) | % | Δ_{min}^2 | β_{SN} | % | Δ_{min}^2 |
| 5×10^8 | 19 | 0.29 | 5×10^3 | 33 | 0.50 | 5×10^4 | 52 | 0.50 | 10^6 | 21 | 3.26 | 4.83 | 41 | 0.29 |
| 5×10^9 | 40 | 0.12 | 5×10^2 | 46 | 0.12 | 5×10^3 | 69 | 0.12 | 10^7 | 42 | 0.13 | 9.65 | 40 | 0.28 |
| 5×10^{10} | 47 | 0.12 | 5×10^1 | 40 | 0.29 | 5×10^2 | 40 | 0.29 | 10^8 | 42 | 0.12 | 19.3 | 25 | 0.12 |
| | | | 5×10^0 | 26 | 0.56 | 5×10^1 | 4 | 6.85 | | | | | | |
| | | | 5×10^{-1} | 19 | 0.74 | 5×10^0 | 0 | 8.74 | | | | | | |
| LMC | | | | | | | | | | | | | | |
| 5×10^8 | 15 | 0.66 | 5×10^3 | 56 | 1.17 | 5×10^4 | 19 | 4.44 | 10^6 | 5 | 2.56 | 4.83 | 31 | 1.17 |
| 5×10^9 | 28 | 0.48 | 5×10^2 | 33 | 0.48 | 5×10^3 | 54 | 0.48 | 10^7 | 38 | 0.48 | 9.65 | 33 | 0.66 |
| 5×10^{10} | 38 | 0.48 | 5×10^1 | 22 | 0.80 | 5×10^2 | 40 | 0.66 | 10^8 | 38 | 0.66 | 19.3 | 17 | 0.48 |
| | | | 5×10^0 | 20 | 0.66 | 5×10^1 | 0 | 11.8 | | | | | | |
| | | | 5×10^{-1} | 15 | 0.66 | 5×10^0 | 0 | 32.7 | | | | | | |
| SMC | | | | | | | | | | | | | | |
| 5×10^8 | 4 | 6.35 | 5×10^3 | 19 | 2.34 | 5×10^4 | 0 | 16.9 | 10^6 | 0 | 21.0 | 4.83 | 5 | 4.92 |
| 5×10^9 | 9 | 4.92 | 5×10^2 | 11 | 4.92 | 5×10^3 | 15 | 2.34 | 10^7 | 2 | 5.20 | 9.65 | 12 | 2.34 |
| 5×10^{10} | 12 | 2.34 | 5×10^1 | 6 | 6.35 | 5×10^2 | 15 | 4.92 | 10^8 | 22 | 2.34 | 19.3 | 7 | 2.83 |
| | | | 5×10^0 | 6 | 6.79 | 5×10^1 | 0 | 9.22 | | | | | | |
| | | | 5×10^{-1} | 4 | 6.97 | 5×10^0 | 0 | 9.93 | | | | | | |

Note: For the graphite fraction and α_C , we adopt the values in Table 4.

α_C may be the consequence of introducing an AC species.

Pei (1992), Weingartner & Draine (2001) and Li et al. (2006) suggested a very small graphite-to-silicate mass ratio to fit the bumpless SMC extinction curve. Their models are in line with our conclusion that an enhanced destruction efficiency of carbonaceous dust relative to silicate better reproduces the SMC extinction curve. However, in our model, the abundance of small carbonaceous grain is inevitably kept to a level at which the 2175 Å bump still appears. thus, we needed to introduce another carbonaceous species (i.e. AC) which does not have such a feature.

4.4 Can we explain all with the same parameter set?

Using our models, we have made an attempt to explain all the well studied extinction curves in the local Universe. Here, we examine a possibility that the three extinction curves are understood as a single evolutionary sequence.

As shown above, the SMC extinction curve has the severest constraint on parameters, with only 20 parameter sets fitting the observational data with $\Delta^2 \leq 8$. Using these 20 parameter sets, we predict the MW and LMC extinction curves to see if they fit these extinction curves as well. We adopt the tuned graphite fraction and α_C listed in Table 4. As a consequence, there are 11 parameter sets (5 per cent of all the 243 sets) fitting extinction curves of the MW, LMC and SMC satisfactorily ($\Delta^2 \leq 8$) at appropriate metallicities $Z = 1.0, 0.5$ and $0.2 Z_\odot$, respectively. Fig. 12 shows an example out of the 11 parameter sets. Although we do not intend to argue that all the galaxies have the

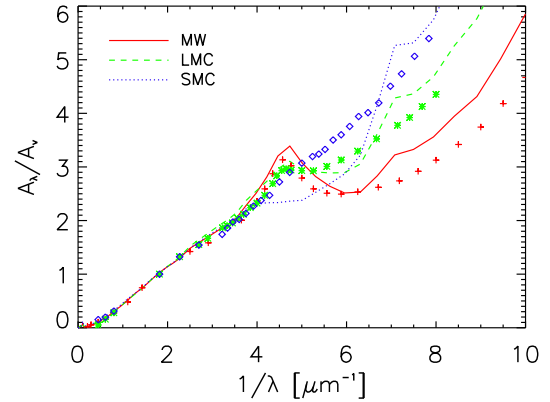


Fig. 12. Metallicity sequence of extinction curves at 0.2, 0.5, and 1 Z_\odot calculated by a single common parameter set (the fiducial parameters in Table 2), compared with the SMC, LMC, and MW extinction curves, respectively. For α_C and the carbonaceous material, we adopt the models in Table 4. Cross, star and square symbols represent the observed mean extinction curves of the MW, the LMC and the SMC taken from Pei (1992). Solid, dashed, and dotted lines are the modeled extinction curves for the MW, the LMC and the SMC.

same dust processing time-scales, we emphasize that we have succeeded in explaining the three well known extinction curves with a single dust evolution framework.

4.5 Extinction curves in other galaxies

We have concentrated on the local extinction curves which are studied in details. Moreover, since the extinction curves are de-

rived for individual lines of sight toward single stars, extinction curves likely reflect the dust properties in the ISM with minor contribution from radiative transfer effects. For example, the Calzetti extinction curve (Calzetti et al. 1994) represents an effective extinction as a result of radiative transfer (absorption and scattering) effects of light emitted from multiple stellar populations (see also Inoue 2005). Extinction curves derived for galaxies whose stars cannot be resolved have in principle the same problem. Careful radiative transfer modeling would be necessary in such a case and is left for future work.

In the distant Universe, quasars and gamma-ray bursts are suitable to derive the extinction curves in their host galaxies because of their simple power-law-like spectral shapes (Maiolino et al. 2004; Stratta et al. 2007; Li et al. 2008; Elíasdóttir et al. 2009; Gallerani et al. 2010; Perley et al. 2010; Zafar et al. 2010, 2011, 2015; Schady et al. 2012). Moreover, they are very bright point sources. Therefore, their extinction curves likely reflect the intrinsic dust properties in the host galaxies, although we should keep in mind that radiative transfer effects, especially scattering, skew the shape of the extinction curve if we deal with highly extinguished objects (e.g. Scicluna & Siebenmorgen 2015). A successful fit to the extinction curve of a quasar at $z = 6.2$ is given by Nozawa et al. (2015), who used their evolution model of grain size distribution. Using our models, we will further examine the diverse types of extinction curves actually observed in those high-redshift objects in the future.

5 conclusion

Using the dust evolution model developed in our previous work, we investigated if the extinction curves in the local galaxies can be explained by well known dust enrichment processes. In order to make a parameter survey possible, we adopted the two-size approximation in which the full range of grain sizes is represented by the small and large sizes divided at $a \sim 0.03 \mu\text{m}$. We considered two dust species, carbonaceous dust and silicate, and calculated the evolution of the large and small grain abundances for each species. For the processes driving the evolution of dust, we considered dust condensation in stellar ejecta, destruction in SN shocks, fragmentation by shattering and growth by coagulation and accretion. To calculate the MW extinction curves, we adopted ‘standard’ dust composition, silicate and graphite. Since the model is computationally light, we surveyed the reasonable ranges for the time-scale of each process and consequently found 37 per cent of the parameter sets fitting the observed MW extinction curve. This means that the known processes driving the evolution of dust successfully reproduces the dust properties consistent with the MW extinction curve. We also showed that the extinction curves are sensitive to the star formation, coagulation and accretion processes.

The same dust evolution model failed to reproduce the SMC extinction curves. This is because the 2175 Å bump feature remains for any parameter set. We proposed two possible modifications: using AC instead of graphite for carbonaceous dust and/or adjusting SN destruction efficiency for small carbonaceous grains. Using AC for carbonaceous dust or adopting a higher SN destruction rate for small carbonaceous dust ($\alpha_C = 0.1$), we found some cases where the extinction curve fits the observed SMC extinction curve. Adopting both modifications at the same time, the fitting improved; in particular, since small carbonaceous dust inevitably remains because of accretion (recall that accretion selectively occurs for small grains), assuming graphite always leads to a significant 2175 Å feature. Thus, considering grain species other than graphite is essential in explaining the SMC extinction curve. We also confirmed that the LMC extinction curve is explained by an intermediate value of $\alpha_C (= 0.2)$ and a mixture of AC and graphite for the carbonaceous component.

By analyzing the favored parameter sets by each extinction curve, we obtained constraint on coagulation and accretion processes. Overall, strong coagulation ($\beta_{\text{co},0} \gtrsim 500$, which means that the coagulation time-scale under the MW dust-to-gas ratio is shorter than $1/500$ of the star-formation time-scale) is favored, especially for the MW. Efficient grain growth by accretion under long cloud lifetimes ($\tau_{\text{cl}} \sim 10^7\text{--}10^8$ yr) fits the observed extinction curves in all the three galaxies, especially the SMC. Longer star formation time-scales than 10^9 yr is also preferred, which is consistent with the picture that those three galaxies have been built up on time-scales comparable to the cosmic age. Other processes are not constrained strongly by observed extinction curves, which implies that they do not have as large a imprint in the dust evolution as accretion and coagulation. Finally, we also presented a possibility of explaining all the three extinction curves as a sequence of metallicity evolution.

Acknowledgments

We thank the anonymous referee for useful comments. We are grateful to Typhoon Lee and You-Hua Chu for their support of KCH’s PhD program. We also thank Kentaro Nagamine, Shohei Aoyama, Ikkoh Shimizu and Peter Scicluna for stimulating discussions. HH is supported by the Ministry of Science and Technology (MoST) grant 105-2112-M-001-027-MY3. MJM acknowledges the support of the UK Science and Technology Facilities Council, the Royal Society of Edinburgh International Exchange Program and the hospitality of the Academia Sinica Institute of Astronomy and Astrophysics.

Appendix 1 Correlation plots for the LMC and SMC

We show the correlation plots for the LMC and SMC. They are produced in the same way as the MW case in Section 4.2 but using the tuned parameters listed in Table 4.

Appendix. References

- Amari S., Lewis R. S., Anders E., 1994, *Geochim. Cosmochim. Acta*, 58, 459
- Asano R. S., Takeuchi T. T., Hirashita H., Nozawa T., 2013, *MNRAS*, 432, 637
- Asano R. S., Takeuchi T. T., Hirashita H., Nozawa T., 2014, *MNRAS*, 440, 134
- Bekki K., Hirashita H., Tsujimoto T., 2015, *ApJ*, 810, 39
- Bianchi S., Schneider R., 2007, *MNRAS*, 378, 973
- Bohren C. F., Huffman D. R., 1983, *Absorption and scattering of light by small particles*
- Calzetti D., Kinney A. L., Storchi-Bergmann T., 1994, *ApJ*, 429, 582
- Cazaux S., Spaans M., 2004, *ApJ*, 611, 40
- Draine B. T., Li A., 2007, *ApJ*, 657, 810
- Dwek E., Scalo J. M., 1980, *ApJ*, 239, 193
- Dwek E., Galliano F., Jones A. P., 2007, *ApJ*, 662, 927
- Elíasdóttir Á., et al., 2009, *ApJ*, 697, 1725
- Fitzpatrick E. L., 1985, *ApJ*, 299, 219
- Fitzpatrick E. L., Massa D., 2007, *ApJ*, 663, 320
- Gall C., Andersen A. C., Hjorth J., 2011, *A&A*, 528, A13
- Gall C., et al., 2014, *Nature*, 511, 326
- Gallerani S., et al., 2010, *A&A*, 523, A85
- Gauger A., Balega Y. Y., Irrgang P., Osterbart R., Weigelt G., 1999, *A&A*, 346, 505
- Gordon K. D., Clayton G. C., Misselt K. A., Landolt A. U., Wolff M. J., 2003, *ApJ*, 594, 279
- Gordon K. D., et al., 2014, *ApJ*, 797, 85
- Groenewegen M. A. T., 1997, *A&A*, 317, 503
- Heger A., Fryer C. L., Woosley S. E., Langer N., Hartmann D. H., 2003, *ApJ*, 591, 288
- Hirashita H., 2015, *MNRAS*, 447, 2937
- Hirashita H., Kuo T.-M., 2011, *MNRAS*, 416, 1340
- Hirashita H., Yan H., 2009, *MNRAS*, 394, 1061
- Hoppe P., Zinner E., 2000, *J. Geophys. Res.*, 105, 10371
- Inoue A. K., 2005, *MNRAS*, 359, 171
- Inoue A. K., 2011, [*Earth, Planets, and Space*], 63, 1027
- Jones A. P., 2009, in Henning T., Grün E., Steinacker J., eds, *Astronomical Society of the Pacific Conference Series Vol. 414, Cosmic Dust - Near and Far*. p. 473
- Jones A. P., Nuth J. A., 2011, *A&A*, 530, A44
- Karakas A. I., 2010, *MNRAS*, 403, 1413
- Kim S.-H., Martin P. G., Hendry P. D., 1994, *ApJ*, 422, 164
- Kobayashi C., Umeda H., Nomoto K., Tominaga N., Ohkubo T., 2006, *ApJ*, 653, 1145
- Korn A. J., Becker S. R., Gummertsbach C. A., Wolf B., 2000, *A&A*, 353, 655
- Kuo T.-M., Hirashita H., 2012, *MNRAS*, 424, L34
- Li A., Draine B. T., 2001, *ApJ*, 554, 778
- Li A., Misselt K. A., Wang Y. J., 2006, *ApJL*, 640, L151
- Li A., Liang S. L., Kann D. A., Wei D. M., Klose S., Wang Y. J., 2008, *ApJ*, 685, 1046
- Liffman K., Clayton D. D., 1989, *ApJ*, 340, 853
- Maiolino R., Schneider R., Oliva E., Bianchi S., Ferrara A., Mannucci F., Pedani M., Roca Sogorb M., 2004, *Nature*, 431, 533
- Mancini M., Schneider R., Graziani L., Valiante R., Dayal P., Maio U., Ciardi B., Hunt L. K., 2015, *MNRAS*, 451, L70
- Marassi S., Schneider R., Limongi M., Chieffi A., Bocchio M., Bianchi S., 2015, *MNRAS*, 454, 4250
- Mathis J. S., Rimpl W., Nordsieck K. H., 1977, *ApJ*, 217, 425
- Mattsson L., De Cia A., Andersen A. C., Zafar T., 2014, *MNRAS*, 440, 1562
- Meixner M., et al., 2010, *A&A*, 518, L71
- Michałowski M. J., 2015, *A&A*, 577, A80
- Michałowski M. J., Murphy E. J., Hjorth J., Watson D., Gall C., Dunlop J. S., 2010a, *A&A*, 522, A15
- Michałowski M. J., Watson D., Hjorth J., 2010b, *ApJ*, 712, 942
- Norris B. R. M., et al., 2012, *Nature*, 484, 220
- Nozawa T., Fukugita M., 2013, *ApJ*, 770, 27
- Nozawa T., Kozasa T., Habe A., Dwek E., Umeda H., Tominaga N., Maeda K., Nomoto K., 2007, *ApJ*, 666, 955
- Nozawa T., Asano R. S., Hirashita H., Takeuchi T. T., 2015, *MNRAS*, 447, L16
- O'Donnell J. E., Mathis J. S., 1997, *ApJ*, 479, 806
- Omukai K., Tsuribe T., Schneider R., Ferrara A., 2005, *ApJ*, 626, 627
- Pei Y. C., 1992, *ApJ*, 395, 130
- Perley D. A., et al., 2010, *MNRAS*, 406, 2473
- Rouillé G., Jäger C., Krasnokutski S. A., Krebsz M., Henning T., 2014, [*Faraday Discussions*], 168, 449
- Russell S. C., Dopita M. A., 1992, *ApJ*, 384, 508
- Sarangi A., Cherkneff I., 2015, *A&A*, 575, A95
- Schady P., et al., 2012, *A&A*, 537, A15
- Schaerer D., Boone F., Zamojski M., Staguhn J., Dessauges-Zavadsky M., Finkelstein S., Combes F., 2015, *A&A*, 574, A19
- Schneider R., Omukai K., Inoue A. K., Ferrara A., 2006, *MNRAS*, 369, 1437
- Schneider R., Valiante R., Ventura P., dell'Agli F., Di Criscienzo M., Hirashita H., Kemper F., 2014, *MNRAS*, 442, 1440
- Scicluna P., Siebenmorgen R., 2015, *A&A*, 584, A108
- Scicluna P., Siebenmorgen R., Wesson R., Blommaert J. A. D. L., Kasper M., Voshchinnikov N. V., Wolf S., 2015, *A&A*, 584, L10
- Stratta G., Maiolino R., Fiore F., D'Elia V., 2007, *ApJL*, 661, L9
- Tinsley B. M., 1980, *Fund. Cosmic Phys.*, 5, 287
- Valiante R., Schneider R., Bianchi S., Andersen A. C., 2009, *MNRAS*, 397, 1661
- Valiante R., Schneider R., Salvadori S., Bianchi S., 2011, *MNRAS*, 416, 1916
- Ventura P., et al., 2012, *MNRAS*, 424, 2345
- Weingartner J. C., Draine B. T., 2001, *ApJ*, 548, 296
- Yajima H., Nagamine K., Thompson R., Choi J.-H., 2014, *MNRAS*, 439, 3073
- Yamasawa D., Habe A., Kozasa T., Nozawa T., Hirashita H., Umeda H., Nomoto K., 2011, *ApJ*, 735, 44
- Yasuda Y., Kozasa T., 2012, *ApJ*, 745, 159
- Zafar T., Watson D. J., Malesani D., Vreeswijk P. M., Fynbo J. P. U., Hjorth J., Levan A. J., Michałowski M. J., 2010, *A&A*, 515, A94
- Zafar T., Watson D., Fynbo J. P. U., Malesani D., Jakobsson P., de Ugarte Postigo A., 2011, *A&A*, 532, A143

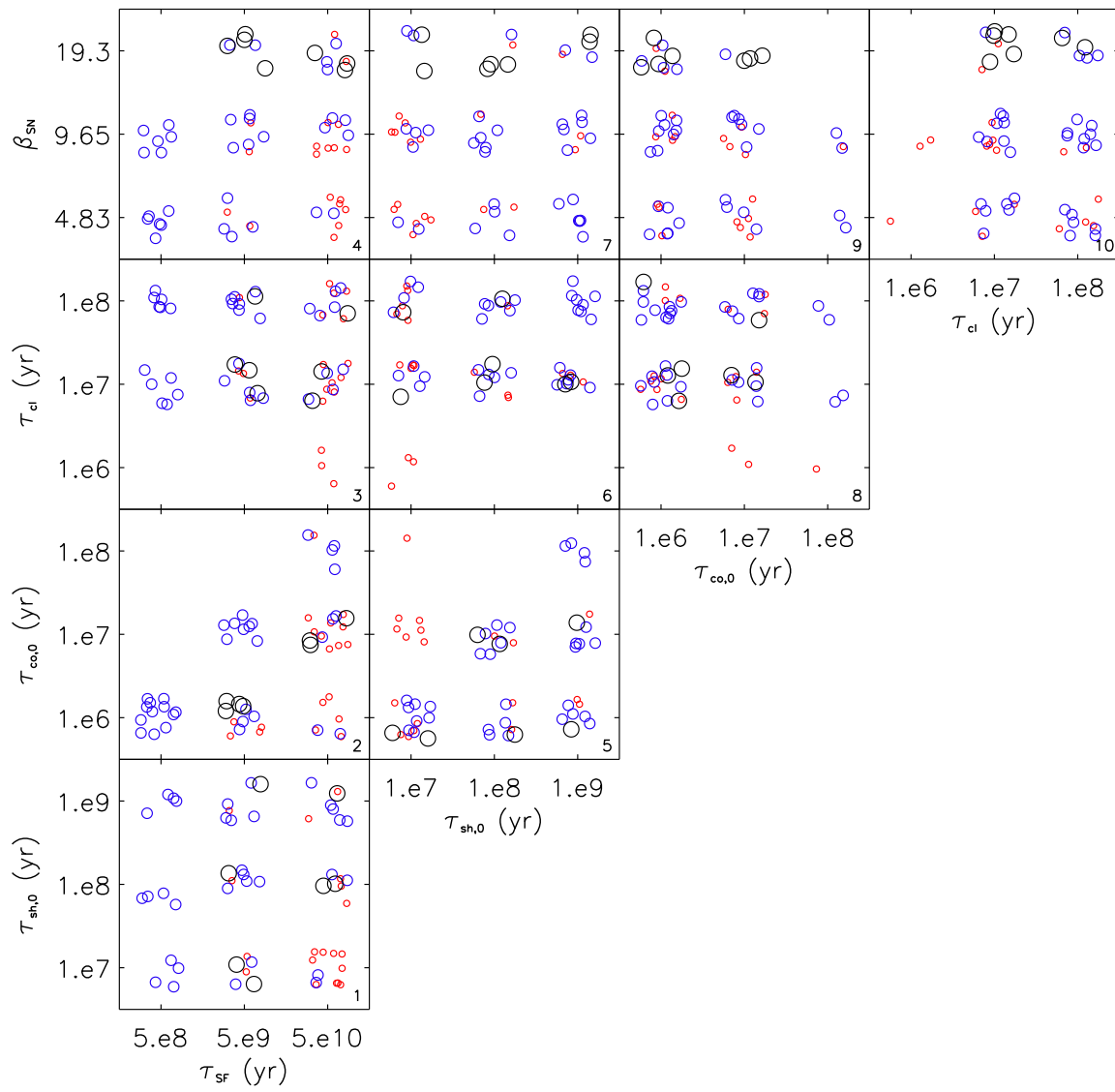


Fig. 13. Same as Fig. 11 but for the LMC.

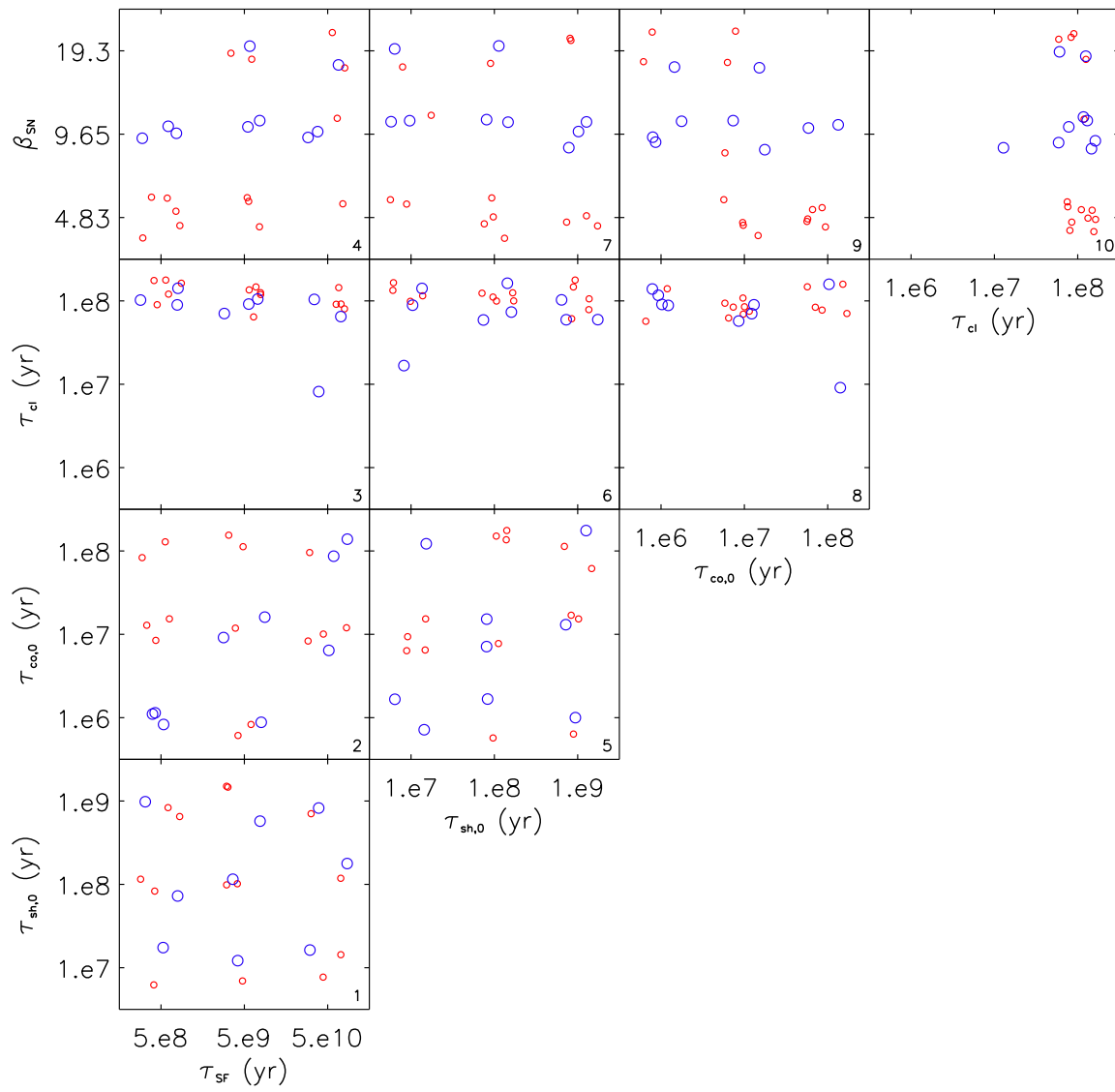


Fig. 14. Same as Fig. 11 but for the SMC.

Zafar T., et al., 2015, *A&A*, 584, A100

Zhukovska S., Henning T., 2013, *A&A*, 555, A99

Zhukovska S., Gail H.-P., Tieloff M., 2008, *A&A*, 479, 453

Zubko V. G., Mennella V., Colangeli L., Bussoletti E., 1996, *MNRAS*,
282, 1321

Zubko V., Dwek E., Arendt R. G., 2004, *ApJS*, 152, 211